Theoretical Study of Ultrafast Photoinduced Electron Transfer Processes in Mixed-Valence Systems

Haobin Wang*

Department of Chemistry and Biochemistry, MSC 3C, New Mexico State University, Las Cruces, New Mexico 88003

Michael Thoss*

Theoretische Chemie, Technische Universität München, D-85747 Garching, Germany

Received: October 21, 2002; In Final Form: December 5, 2002

The recently proposed self-consistent hybrid method is applied to study photoinduced electron transfer (ET) reactions in mixed-valence compounds $(NH_3)_5Ru^{III}NCRu^{II}(CN)_5^-$ and $(NH_3)_5Ru^{III}NCFe^{II}(CN)_5^-$ in solution. To describe these ET processes in the condensed phase, both intramolecular modes (inner sphere) and the solvent environment (outer sphere) are taken into account using a model that is based on the analysis of experimental optical line shapes. The dynamics of the back ET process after photoexcitation is studied in detail. In particular we investigate the effects of intramolecular vibrational modes and solvent dynamics, as well as the influence of important physical parameters such as the electronic coupling and the temperature. In qualitative agreement with results of time-resolved optical experiments, the simulations predict an ultrafast decay of the population of the charge-transfer state. Oscillatory features are observed superimposed on the population decay, and their relations to electronic and vibrational coherence effects are discussed. Furthermore, we present comparisons with results of approximate methods such as golden rule type perturbation theory and the classical Ehrenfest model, demonstrating the necessity of using accurate quantum dynamical simulation methods to study intervalence electron-transfer processes.

I. Introduction

Recent advances in femtosecond nonlinear spectroscopic techniques have fostered considerable interest in theoretical studies of ultrafast chemical reactions occurring in complex environments. Among these, ultrafast photoinduced electron transfer (ET) processes, which often take place on a subpicosecond time scale, have attracted special attention. Besides the well-studied role of thermal ET as an elementary step in many chemical and biological reactions,[1−3] photoinduced ultrafast ET processes often reveal additional interesting features. In time-resolved optical experiments it has been demonstrated that in these ET reactions both the coupling to intramolecular modes of the solute (inner sphere) and that to the solvation dynamics (outer sphere) can have significant impacts on the ET dynamics.[2,4−8] Furthermore, observations of (seemingly) multi-exponential relaxation processes and oscillatory features in ultrafast spectroscopic signals for several ET reactions[6−13] have raised important questions about the nature of the ET dynamics as well as the occurrence and observability of electronic and vibrational quantum coherence in a condensed phase environment.

Mixed-valence compounds with two metal centers, such as the compounds $(NH_3)_5Ru^{III}NCRu^{II}(CN)_5^-$ (for simplicity we denote this compound as RuRu) and $(NH_3)_5Ru^{III}NCFe^{II}(CN)_5^-$ (denoted as RuFe), provide a particularly interesting class of ET systems for studying these phenomena.[5,7,8,10,14−19] The generic metal−metal charge-transfer (MMCT) process in these two systems can be schematically represented as

$$(NH_3)_5Ru^{III}NCRu^{II}(CN)_5^- \underset{ET}{\overset{h\nu}{\rightleftharpoons}} (NH_3)_5Ru^{II}NCRu^{III}(CN)_5^- \quad (1.1a)$$

$$(NH_3)_5Ru^{III}NCFe^{II}(CN)_5^- \underset{ET}{\overset{h\nu}{\rightleftharpoons}} (NH_3)_5Ru^{II}NCFe^{III}(CN)_5^- \quad (1.1b)$$

Upon photoexcitation into the MMCT band an electron is transferred from one metal center to another. This process is followed by an ultrafast internal conversion, resulting in the back transfer of the electron on a subpicosecond time scale.[7,8,15] The study of these particular ET reactions are of interest for both experimental and theoretical reasons: First, in femtosecond pump−probe studies of these ET reactions in solution, coherent oscillations have been observed on time scales longer than the ET time, suggesting that the coherence of the vibrational motion is maintained during the ET process.[7,8,15] Second, the observation of multiple time scales in optical signals indicates that the ET process cannot be characterized by a simple exponential decay. This is often attributed to the existence of multiple time scales in the solvation dynamics, as well as the influence of the strongly bound ligand modes. Therefore, golden rule type approaches may not be applicable (vide infra). Finally, modelings of these ET reactions are relatively straightforward since they correspond to direct optical ET and, therefore, most of the parameters required can be obtained from the analysis of absorption and resonance Raman spectra.

Despite these considerations, there have been relatively few theoretical studies of the dynamics of these intervalence ET

* Corresponding authors. Fax: (505) 646-2649; e-mail: whb@intrepid.nmsu.edu (H.W.). Fax: 49-89-2891-3622; e-mail: michael.thoss@ch.tum.de (M.T.).

10.1021/jp0272668 CCC: $25.00
Published on Web 03/12/2003

reactions.[15,48,49] The major challenge for a simulation of these reactions is to accurately describe the quantum mechanical effect of the nuclear degrees of freedom and their interactions with the electronic states during the ET process. This requires a proper treatment of both the strongly coupled intramolecular modes and the solvent degrees of freedom. Well-known mixed quantum classical approaches, such as the classical Ehrenfest model [sometimes referred to as the classical path or the time-dependent self-consistent field (TDSCF) model][20−26] or the surface-hopping method,[27−30] usually treat the nuclear degrees of freedom purely classically, and thus completely neglect quantum interference effects between the electronic and nuclear degrees of freedom. On the other hand, many approximate quantum theories, e.g., the noninteracting blip approximation[31,32] or Redfield theory,[32−38] are based on the perturbative treatment of electronic or nuclear couplings which is only valid at certain physical regimes. Furthermore, these approaches tend to assume a well-defined time scale separation between electronic and nuclear degrees of freedom. As a consequence, only the short-time quantum effect of the environment can be described accurately. A similar problem exists in path integral approaches based on the Feynman−Vernon influence functional[39] where, within the linear response model, the harmonic bath is integrated out.[32,40−47] In contrast to nonadiabatic ET reactions with a relatively fast decay of the bath correlation functions, the influence of the nuclear environment (i.e., the "memory" effect of the bath), in the mixed-valence ET reactions considered here, may persist throughout the entire ET process, thus rendering a path integral calculation beyond the short-time dynamics unfeasible.[48]

In a previous paper[49] we have presented preliminary studies of the quantum dynamics of the photoinduced ET reactions in the RuRu compound in solution, using the numerically exact self-consistent hybrid method.[50,51] This study was motivated by the work of Barbara, Hupp, and co-workers,[4,15,19] who have analyzed the MMCT band shape for the RuRu/RuFe systems and used a hybrid of the classical ET model of Sumi and Marcus[52] and the vibronic ET model of Jortner and Bixon[53] to describe the multiexponential population decay of the charge-transfer state after photoexcitation. We have shown that the self-consistent hybrid method is able to accurately describe the ET dynamics in such mixed-valence systems over a relatively long time scale. In qualitative agreement with experiments, our simulations presented in ref 49 predict that the ET dynamics for the RuRu system are characterized by a bimodal decay of the charge-transfer state and are significantly influenced by both intramolecular vibrational modes and solvation dynamics. The former manifests itself in oscillatory features superimposed on the population decay, and the latter results in a dynamic solvent effect.

Extending our previous work, in the present paper we report a detailed study of photoinduced ET reactions in the RuRu and RuFe compounds in solution. Specifically, we investigate the dependence of the population dynamics of the charge-transfer state on the time scales of the solvation dynamics, as well as on physical parameters such as the temperature and the electronic coupling. Furthermore, we will analyze the important role of intramolecular modes (inner sphere) in the overall ET dynamics. The remaining part of the paper is organized as follows: section II introduces the model used in our theoretical study. The basic idea of the simulation method and some details of the convergence procedure are described in section III. Section IV presents results of numerical simulations for different parameter regimes, as well as a detailed discussion of their physical implications. Section V summarizes and concludes.

II. Model of the Electron-Transfer Reactions in the $(NH_3)_5Ru^{III}NCRu^{II}(CN)_5^-$ and $(NH_3)_5Ru^{III}NCFe^{II}(CN)_5^-$ Systems

As described previously,[49] our model for describing the photoinduced ET dynamics in the RuRu and RuFe systems is based on the line-shape analysis of Hupp, Barbara, and co-workers.[7,15,19] Two diabatic electronic states are taken into account: the electronic ground state $|\phi_1\rangle$ and the charge-transfer state $|\phi_2\rangle$, which results from the photoinduced ET between the metal centers. The coupling of the electronic states to the nuclear degrees of freedom is described by contributions from an inner sphere and an outer sphere. The former includes Raman-active intramolecular modes of the RuRu/RuFe compounds, and the latter models the solvation dynamics of a particular solvent. Due to the ultrafast time scales (subpicosecond) for the ET dynamics in the RuRu and RuFe systems, it is expected that the inner-sphere vibrational modes play an important role in the ET process.

According to these considerations, the Hamiltonian can be written in the form

$$\hat{H} = |\phi_1\rangle E_1\langle\phi_1| + |\phi_2\rangle E_2\langle\phi_2| + |\phi_1\rangle V\langle\phi_2| + |\phi_2\rangle V\langle\phi_1| + H_N \tag{2.1}$$

$$H_N = H_v + H_B \tag{2.2}$$

The electronic parameters of the Hamiltonian are determined by the free-energy difference $\Delta G = E_2 - E_1$ and the coupling V between the two electronic states. The latter is assumed to be approximately independent of the vibrational degrees of freedom. The nuclear Hamiltonian H_N contains two parts, H_v and H_B. H_v describes the intramolecular modes included in the model within the harmonic approximation

$$H_v = \frac{1}{2}\sum_j \left[P_j^2 + \Omega_j^2 \left(X_j - |\phi_2\rangle \frac{c_j}{\Omega_j^2} \langle\phi_2|\right)^2 \right] \tag{2.3}$$

Here, X_j and P_j denote the mass-scaled coordinate and momentum of the jth mode with frequency Ω_j and coupling strength c_j. In the context of ET the latter is usually specified by the reorganization energy $\lambda_j = c_j^2/(2\Omega_j^2)$. The electronic parameters as well as frequencies and reorganization energies of the intramolecular modes have been adopted from the model of Barbara and co-workers and are given in Tables 1 and 2.[54] These parameters, unless specified otherwise, are used in our dynamical simulations. For an assignment of the corresponding normal modes see ref 15.

The influence of the solvent on the ET dynamics is modeled, within linear response theory, by a linear coupling to a bath of harmonic oscillators[32,55,56]

$$H_B = \frac{1}{2}\sum_l \left[p_l^2 + \omega_l^2 \left(x_l - |\phi_2\rangle \frac{d_l}{\omega_l^2} \langle\phi_2|\right)^2 \right] \tag{2.4}$$

The parameters of the solvent part of the nuclear Hamiltonian (H_B) are characterized by its spectral density[31,32]

$$J_B(\omega) = \frac{\pi}{2}\sum_l \frac{d_l^2}{\omega_l} \delta(\omega - \omega_l) \tag{2.5}$$

TABLE 1: Parameters of the Model Hamiltonian (eq 2.1) for the RuRu Compound, Including Vibrational Frequencies Ω_j and Reorganization Energies λ_j of the Intramolecular Modes as Well as Electronic Free Energy Gap $E_2 - E_1$ and Diabatic Coupling V (Adopted from Refs 7 and 15)[a]

j	Ω_j	λ_j	no. of basis functions
1	2118	484	8
2	2077	135	4
3	565	313	12
4	539	363	10
5	492	189	7
6	470	107	6
7	355	95	6
8	270	483	20
9	160	500	31
	$E_2 - E_1 = 7880$		$V = 1500$

[a] All quantities are given in cm^{-1}. The last column specifies the number of primitive basis functions used in our simulations.

TABLE 2: Same as Table 1, but for the RuFe System

j	Ω_j	λ_j	no. of basis functions
1	2104	563	9
2	2060	50	3
3	603	537	13
4	544	134	6
5	482	164	7
6	468	90	6
7	361	74	5
8	270	468	16
9	160	500	28
	$E_2 - E_1 = 3930$		$V = 1500$

which is related to the (classical) bath energy-gap correlation function $C_B(t)$ via

$$C_B(t) \sim \frac{1}{\pi}\int_0^\infty d\omega \, \frac{J_B(\omega)}{\omega} \cos(\omega t) \tag{2.6}$$

For some systems $C_B(t)$ can be obtained from classical molecular dynamics simulations.[57,58] Here, we take a more phenomenological approach based on recent experimental and theoretical observations that the solvation dynamics in many polar solvents involve typically (at least) two important time scales:[59,60] an ultrafast inertial decay of Gaussian character and a slower diffusive decay of exponential form. Accordingly, we model the bath by a bimodal spectral density

$$J_B(\omega) = J_G(\omega) + J_D(\omega) \tag{2.7}$$

with a Gaussian part accounting for the ultrafast inertial decay

$$J_G(\omega) = \sqrt{\pi}\frac{\lambda_G \omega}{\omega_G} e^{-[\omega/(2\omega_G)]^2} \tag{2.8a}$$

and a Debye part describing the slower diffusive decay

$$J_D(\omega) = 2\lambda_D \frac{\omega\omega_D}{\omega^2 + \omega_D^2} \tag{2.8b}$$

The corresponding classical energy-gap correlation function $C_B(t)$ is then given by

$$C_B(t) \sim \lambda_G e^{-(t/\tau_G)^2} + \lambda_D e^{-t/\tau_D} \tag{2.9}$$

where we have introduced the solvent relaxation times $\tau_G = 1/\omega_G$ and $\tau_D = 1/\omega_D$. The coupling strengths of the two parts of the spectral density are specified by the corresponding reorganization energies λ_G and λ_D, respectively. Both the reorganization energies and the relaxation times depend on the specific solvent to be considered. In the calculations presented below we have chosen default values of $\lambda_G = 2240\ cm^{-1}$ and $\lambda_D = 960\ cm^{-1}$,[61] corresponding to a situation where the inertial Gaussian decay constitutes 70% of the total relaxation, similar to those found for solvation in acetonitrile and water.[59] The default relaxation times of the solvent are $\tau_G = 53$ fs and $\tau_D = 530$ fs, corresponding to $\omega_G = 100\ cm^{-1}$ and $\omega_D = 10\ cm^{-1}$, and have been chosen to mimic a fast relaxing solvent. In some of the results presented in section IV, these parameters are also treated as variable parameters to study the influence of the solvent relaxation time scale on the ET dynamics.

The solvent spectral density of eq 2.7 can be discretized to the form of eq 2.5 via the relation

$$d_l^2 = \frac{2}{\pi}\omega_l \frac{J_B(\omega_l)}{\rho(\omega_l)} \tag{2.10a}$$

where $\rho(\omega)$ is a density of frequencies satisfying

$$\int_0^{\omega_l} d\omega \, \rho(\omega) = l, \quad l = 1, ..., N_B \tag{2.10b}$$

with N_B the number of solvent modes in the simulation. The precise functional form of $\rho(\omega)$ does not affect the final answer if enough modes are included, but it does affect the efficiency of solving the problem (i.e., the number of modes needed to represent the continuum). Here we choose $\rho(\omega)$ to accurately reproduce the reorganization energy, i.e.

$$\rho(\omega) = a\frac{J_B(\omega)}{\omega} \tag{2.11a}$$

where the normalization constant is given by

$$a = \frac{N_B}{\int_0^\infty d\omega \, \frac{J_B(\omega)}{\omega}} \tag{2.11b}$$

These discretized solvent modes are then combined with the intramolecular modes to form the overall nuclear environment.

To illustrate the different time scales of the nuclear degrees of freedom, it is instructive to consider the total (inner sphere + outer sphere) normalized energy-gap correlation function

$$\frac{C(t)}{C(0)} = \frac{\int_0^\infty d\omega \, \frac{J(\omega)}{\omega} \cos(\omega t)}{\int_0^\infty d\omega \, \frac{J(\omega)}{\omega}} \tag{2.12}$$

which is given as the Fourier transform of the overall spectral density

$$J(\omega) = \frac{\pi}{2}\sum_j \frac{c_j^2}{\Omega_j}\delta(\omega - \Omega_j) + J_B(\omega) \tag{2.13}$$

Insertion of eqs 2.7 and 2.8 gives

$$\frac{C(t)}{C(0)} = \lambda^{-1}[\lambda_G e^{-(\omega_G t)^2} + \lambda_D e^{-\omega_D t} + \sum_j \lambda_j \cos(\Omega_j t)] \tag{2.14}$$

where $\lambda = \lambda_G + \lambda_D + \sum_j \lambda_j$ is the total reorganization energy. Figure 1a depicts $C(t)$ for the RuFe system (similar behavior

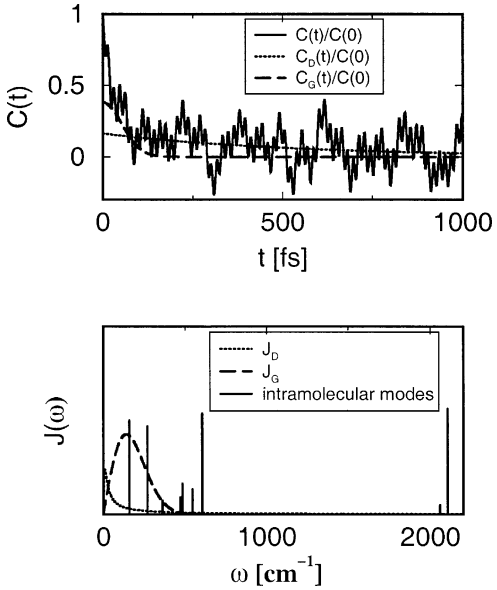

Figure 1. Properties of the nuclear environment for the RuFe system. Upper panel: total (inner sphere + outer sphere) normalized energy-gap correlation function $C(t)/C(0)$ (full line) as well as separate contributions of the Gaussian (dashed line) and the Debye (dotted line) part of the spectral density. Lower panel: Gaussian (dashed line) and Debye (dotted line) part of the spectral density of the bath as well as reorganization energies of the intramolecular vibrational modes.

has also been found for the RuRu system[49]), together with separate contributions from the Gaussian part and the Debye part of the bath spectral density. The corresponding spectral density of the bath and the reorganization energies of the intramolecular modes are illustrated in Figure 1b. It is thus expected that the complicated time scales of $C(t)$ will manifest themselves in the overall ET dynamics for the intervalence systems considered in this paper.

III. Theoretical Method

A. Summary of the Self-Consistent Hybrid Method. In this paper the self-consistent hybrid method[50,51] is applied to study the photoinduced ET dynamics in the RuRu and RuFe systems. This method, which has been proposed recently for simulating quantum dynamics in the condensed phase, is based on an iterative convergence procedure for a dynamical hybrid approach. In this approach the overall system is first partitioned into a *core* and a *reservoir*, based on any convenient initial guess. A dynamical hybrid calculation is then carried out, with the core treated via a numerically exact quantum mechanical method, namely the multiconfiguration time-dependent Hartree (MCTDH) approach,[62,63] and the reservoir treated via a more approximate method, e.g., classical mechanics or quantum perturbation theory. Next, the size of the core, as well as other variational parameters, is systematically increased to achieve numerical convergence for the overall quantum dynamics. The method has been applied to the standard model of ET in polar solvents—the spin-boson model with Debye dielectric relaxation[51]—and a model for electronic resonance decay in the presence of a vibrational bath.[50] More recently, it has been used in a preliminary study of the photoinduced ET dynamics in the RuRu system.[49]

To illustrate the practical procedure for simulating the photoinduced ET dynamics in the condensed phase, let us consider a generic time correlation function of the type (hereafter $\hbar = 1$)

$$C_{AB}(t) = \frac{1}{Q_N}\,\mathrm{tr}[\hat{\rho}_N \hat{A} e^{i\hat{H}t}\hat{B}e^{-i\hat{H}t}] \tag{3.1a}$$

where $\hat{H}$ is given in eq 2.1, $\hat{A}$ and $\hat{B}$ are operators for the electronic degrees of freedom that correspond to some physical quantities (e.g., the reduced density matrix, dipole moment), $\hat{\rho}_N$ is the density operator for the nuclear degrees of freedom, and Q_N denotes the corresponding partition function, i.e.

$$Q_N = \mathrm{tr}\,[\hat{\rho}_N] \tag{3.1b}$$

To study ET dynamics in the condensed phase, the continuous distribution of solvent modes (outer sphere) is first discretized with a finite number of bath modes[50,51,64] as illustrated in the previous section. The number of modes that can adequately represent the continuum depends on the specific physical regime and serves as a convergence parameter. These outer sphere bath modes are then combined with the intramolecular modes (inner sphere) as well as the electronic part to give the total Hamiltonian in eq 2.1.

A rigorous quantum treatment of all degrees of freedom in the trace expression in eq 3.1a is only feasible for a smooth outer-sphere spectral density (without inner sphere) and a very limited parameter regime.[64] Therefore, the self-consistent hybrid method has to be used in the present study. As outlined above, in this approach the overall system is divided into a core and a reservoir, with the total Hamiltonian written as

$$\hat{H} = H_{co}(\hat{p}_s,\hat{s}) + H_{rev}(\hat{p},\hat{q}) + H_I(\hat{p}_s,\hat{s};\hat{p},\hat{q}) \tag{3.2}$$

where $H_{co}(\hat{p}_s,\hat{s})$ and $H_{rev}(\hat{p},\hat{q})$ represent the uncoupled Hamiltonian for the core and the reservoir, respectively, and $H_I(\hat{s},\hat{p}_s;\hat{p},\hat{q})$ represent their interactions. The time evolutions of the core and the reservoir are thus coupled dynamically.

In our applications, the core is treated by the numerically exact time-dependent multiconfiguration self-consistent field (TD-MCSCF) or multiconfiguration time-dependent Hartree (MCTDH)[62,63] method. The approximate method for treating the reservoir should be reasonably accurate and easily implementable. While previously both classical mechanics and quantum perturbation theory have been applied in this context,[50,51] in the present work we choose to use the former. Accordingly, the quantum mechanical trace expression in eq 3.1a is modified as

$$C_{AB}(t) = \frac{1}{Q_N}\int d\mathbf{p}_0 \int d\mathbf{q}_0\, \rho_N^{rev}(\mathbf{p}_0,\mathbf{q}_0)\,\mathrm{tr}[\hat{\rho}_N^{co}\hat{A}e^{i\hat{H}t}\hat{B}e^{-i\hat{H}t}] \tag{3.3}$$

where the trace is now only over the core and the phase space integration is over the reservoir. The initial density operator of the nuclear degrees of freedom, $\hat{\rho}_N$, is split into a core part, $\hat{\rho}_N^{co}$, and a corresponding classical distribution ρ_N^{rev} for the reservoir. Based on a semiclassical description,[65] the initial phase space distribution $\rho_N^{rev}(\mathbf{p}_0,\mathbf{q}_0)$ is obtained by taking the Wigner transform of the corresponding operator $\hat{\rho}_N^{rev}$

$$\rho_N^{rev}(\mathbf{p}_0,\mathbf{q}_0) = \frac{1}{(2\pi)^{N_r}}\int d\Delta\mathbf{q}\; e^{-i\mathbf{p}_0\cdot\Delta\mathbf{q}}\left\langle \mathbf{q}_0 + \frac{\Delta\mathbf{q}}{2}\middle|\hat{\rho}_N^{rev}\middle|\mathbf{q}_0 - \frac{\Delta\mathbf{q}}{2}\right\rangle \tag{3.4}$$

where N_r is the number of reservoir degrees of freedom.

Thus the core comprises the two electronic states and some of the vibrational modes that satisfy certain criteria (e.g., with frequencies $\omega > \omega_q$, where ω_q serves as a convergence parameter[50]). The reservoir comprises the remaining degrees of

freedom. Iterative calculations are then carried out with the core−reservoir partition treated as a convergence parameter. The number of the modes included in the core, as well as other variational parameters, is increased systematically until convergence (usually to within 10% relative error) is reached. If all the modes were treated classically (i.e., the core comprised only the two electronic states), this method would have been equivalent to the standard classical path (Ehrenfest) method. However, because the calculation is converged with respect to the number of modes included in the quantum propagation, the results are in principle numerically exact.

Two types of time correlation functions are considered in this paper. The first is the population of the charge-transfer state after photoexcitation from the ground state:

$$P(t) = \frac{1}{Q_N}\,\mathrm{tr}[e^{-\beta\hat{H}_{N1}}|\phi_2\rangle\langle\phi_2|e^{i\hat{H}t}|\phi_2\rangle\langle\phi_2|e^{-i\hat{H}t}] \tag{3.5}$$

i.e., $\hat{A} = \hat{B} = |\phi_2\rangle\langle\phi_2|$, and $\hat{\rho}_N = e^{-\beta\hat{H}_{N1}}$ in eq 3.1a. Thereby, $\hat{H}_{N1}$ denotes the vibrational Hamiltonian of the intramolecular and the bath modes in the electronic ground state, i.e.

$$\hat{H}_{N1} = \langle\phi_1|\hat{H}_N|\phi_1\rangle = \frac{1}{2}\sum_j (P_j^2 + \Omega_j^2 X_j^2) + \frac{1}{2}\sum_l (p_l^2 + \omega_l^2 x_l^2) \tag{3.6}$$

The other correlation function considered is the dipole correlation function:

$$C_\mu(t) = \frac{1}{Q}\,\mathrm{tr}\{e^{-\beta\hat{H}}[\hat{\mu}(t),\hat{\mu}]\} \tag{3.7a}$$

with

$$\hat{\mu}(t) \equiv e^{i\hat{H}t}\hat{\mu}e^{-i\hat{H}t}, \quad Q = \mathrm{tr}[e^{-\beta\hat{H}}] \tag{3.7b}$$

and

$$\hat{\mu} = |\phi_1\rangle\mu_0\langle\phi_2| + |\phi_2\rangle\mu_0\langle\phi_1| \tag{3.7c}$$

Here, $\hat{\mu}$ denotes the dipole operator, which is assumed to be independent of the vibrational coordinates (Condon approximation). Fourier transform of $C_\mu(t)$ gives the (linear) absorption spectrum $I(\omega)$:

$$I(\omega) \sim \frac{\omega}{2\pi}\int_{-\infty}^{\infty} dt\, e^{i\omega t} C_\mu(t) \tag{3.8}$$

In the applications considered in this paper, there is a relatively large energy difference between the ground state and the photoexcited state. Therefore, we can invoke the approximation

$$e^{-\beta\hat{H}} \simeq e^{-\beta\hat{H}_{N1}}|\phi_1\rangle\langle\phi_1|, \quad Q \simeq \mathrm{tr}[e^{-\beta\hat{H}_{N1}}] \tag{3.9}$$

which corresponds to a factorized initial state.

To evaluate the trace/phase space integration in eq 3.3, we use a Monte Carlo procedure. Both the classical phase space variables $(\mathbf{p}_0,\mathbf{q}_0)$ for the reservoir and the quantum states $\{\mathbf{n}\}$ of the core are randomly selected via an importance sampling procedure which is based on the distribution functions $\rho_N^{rev}(\mathbf{p}_0,\mathbf{q}_0)$ and $\hat{\rho}_N^{co}(\mathbf{n})$, respectively. It is important to note that in the above procedure one does not average over the time-dependent wave functions or quantities related to a single time propagator $e^{-i\hat{H}t}$, which is known to be plagued by the "sign problem". Instead, physical observables that relate to the Heisenberg operator $e^{i\hat{H}t}\hat{B}e^{-i\hat{H}t}$ are averaged. The procedure is thus very similar to a classical Monte Carlo calculation that is free from phase oscillations. For the present application, statistical convergence is usually achieved for a sample size of $\sim 10^2-10^3$.

B. Convergence Procedure for the Self-Consistent Hybrid Method. To obtain accurate results for the photoinduced ET dynamics in RuRu and RuFe systems, convergence tests need to be carried out for the quantum MCTDH treatment of the core, the relative size of the core in the self-consistent hybrid method, and the number of the solvent degrees of freedom used to represent the condensed phase environment. Below, we discuss details of these convergence tests for the RuFe system at $T = 300$ K. A similar procedure has also been carried out for other temperatures and parameter regimes, as well as for the RuRu system.

To examine the vibrational coherence superimposed on the electronic population dynamics, the simulation results have been converged up to 1 ps, a time scale considerably longer than the intrinsic time scale of the electronic and intramolecular vibrational degrees of freedom. The computational cost thus ranges between 1 and 10 CPU hours for each statistical sample, significantly more than the previous study of the spin-boson problem in simpler parameter regimes.[50,51] On the other hand, most of the qualitative features of the ET dynamics can be obtained within the first few hundred femtoseconds and require much less numerical effort.

1. Convergence in the Multiconfiguration Time-Dependent Hartree Method. In the MCTDH method,[62,63] the wave function is expanded in time-dependent Hartree products:

$$|\Psi(t)\rangle = \sum_J A_J(t)|\Phi_J(t)\rangle = \sum_{j_1}\sum_{j_2}\cdots\sum_{j_N} A_{j_1 j_2 \cdots j_N}(t)\prod_{k=1}^{M}|\phi_{j_k}^{k}(t)\rangle \tag{3.10}$$

Here, $|\phi_{j_k}^{k}(t)\rangle$ is the "single-particle" (SP) function for the kth SP degree of freedom and M denotes the number of SP degrees of freedom. Each SP degree of freedom usually contains several (Cartesian) degrees of freedom in our calculation, and for convenience the SP functions within the same SP degree of freedom are chosen to be orthonormal.

The working equations within the MCTDH scheme are[62]

$$i\dot{A}_J(t) = \langle\Phi_J(t)|\hat{H}_c|\Psi(t)\rangle = \sum_L \langle\Phi_J(t)|\hat{H}_c|\Phi_L(t)\rangle A_L(t) \tag{3.11a}$$

$$i|\dot{\underline{\phi}}^k(t)\rangle = \hat{h}_k|\underline{\phi}^k(t)\rangle + (1-\hat{P}^k)(\hat{\rho}^k)^{-1}\langle\hat{H}_c(t)\rangle^k|\underline{\phi}^k(t)\rangle \tag{3.11b}$$

$$\hat{H} = \hat{H}_c + \sum_k \hat{h}_k \tag{3.11c}$$

where all the notations have been given previously.[64] Each SP function $|\phi_n^k(t)\rangle$ is expanded in a chosen time-independent basis set $\{|\varphi_i^k\rangle\}$

$$|\phi_n^{\,k}(t)\rangle = \sum_i c_{i,n}^{\,k}(t)|\varphi_i^{\,k}\rangle \tag{3.12}$$

Note that $|\varphi_i^k\rangle$ is the basis function for an SP degree of freedom, and is thus a direct product of basis functions for all the Cartesian degrees of freedom within the SP group.

In choosing the basis functions for each Cartesian degree of freedom, we use the two diabatic states for the electronic degree of freedom and harmonic oscillator wave functions for the nuclear degrees of freedom. The number of basis functions for each outer sphere bath mode is determined from a thermal criterion, i.e., the highest state included has a Boltzmann

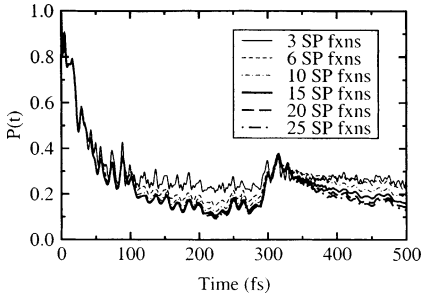

Figure 2. Convergence in the simulation of $P(t)$ at $T = 300$ K for the RuFe system versus number of SP functions for each SP group. For simplicity, only the intramolecular modes are included in the simulation and only results for the first 500 fs are shown.

weighting less than a preset tolerance (e.g., 10^{-4}). For the strongly coupled intramolecular modes, the number of basis functions is primarily determined from their couplings to the electronic degree of freedom. Test calculations are then carried out to ensure the convergence in the number of basis functions. Tables 1 and 2 list the converged choices for the systems considered in the present work.

Several degrees of freedom are then combined together to form one SP. The number of primitive basis functions ($|\varphi_i^k\rangle$) within one SP consists of all possible combinations of the basis functions for each degree of freedom, and is thus a large number. These primitive basis functions, $|\varphi_i^k\rangle$, are then contracted using an adiabatic reduction technique,[66] where states with energies higher than E_{cut} are rejected with E_{cut} a convergence parameter. Such a contraction can significantly reduce the number of necessary basis functions in the calculation as demonstrated in previous applications,[50,51,64] and is essential for practical applications of MCTDH to a large number of degrees of freedom.

The most important convergence test for a MCTDH calculation is the total number of (time-dependent) configurations employed. This is illustrated here for the calculation of the population of the charge-transfer state for the RuFe system, eq 3.5. For demonstration purposes, only the intramolecular modes in Table 2 are included in this convergence test in order to keep the comparisons simple. The final results presented in the next section contain both the intramolecular modes and the outer-sphere solvent modes. Figure 2 shows the convergence of $P(t)$ for the RuFe system at 300 K with respect to increasing the number of SP functions for each SP degree of freedom. Three SP groups are formed using the following combination of intramolecular modes: (1,2,6,7), (3,4,5), (8,9) (the indices are given in Table 2). This particular combination is only for the convenience of carrying out the adiabatic contraction; other ways are also possible but are slightly less efficient. The number of SP functions are the same for all the SP groups. For example, if 10 SP functions are used for each SP degree of freedom, there are a total of $10^3 = 1000$ configurations in the simulation. The calculation to test the convergence is carried out up to $t = 1$ ps with the relative accuracy criteria set to <10%. For graphical clarity, only the first 500 fs are shown in Figure 2.

The short-time dynamics is relatively easy to converge. It can be seen from Figure 2 that three SP functions per each SP group (a total of 27 configurations) give already a reasonable result for the first 100 fs. However, many more configurations are required to converge the longer time dynamics of $P(t)$. Within 1 ps, 20 SP functions per each SP degree of freedom (a total of 8000 configurations) are needed to capture the details of vibrational coherence exhibited in the electronic population. The most pronounced structure is the recurrence at $t \approx 320$ fs. A calculation with a smaller number of configurations misses this feature. The requirement of many SP functions per SP degree of freedom is in contrast to a previous study of the spin-boson problem in simpler parameter regimes,[50,51,64] where three to five SP functions are adequate to obtain converged results. The main reasons for this difference are the strong couplings of the intramolecular modes to the electronic states and the relative large energy difference between the ground state and the photoexcited state. The required number of SP functions for the outer-sphere solvent SP groups, on the other hand, is moderate: three to five SP functions give a converged result in this category, similar to previous cases.[50,51]

In the final simulation of the ET dynamics for the RuFe system at $T = 300$ K, we use 20 SP functions per each intramolecular SP group and four SP functions per each solvent SP group. The numbers are slightly different for simulations at different temperatures. For example, 18 and 22 SP functions are used for each intramolecular SP group at 200 and 500 K, respectively. For the RuRu system, more configurations are needed; e.g., 24 SP functions per each intramolecular SP group are used for $T = 300$ K.

2. Convergence versus the Core−Reservoir Partition. The major difference between the self-consistent hybrid method and other dynamical hybrid methods is that the core−reservoir partition is put into a convergence scheme. To obtain numerically exact results for a particular problem, one needs to make sure that the core part contains all degrees of freedom that are necessary to produce the true quantum dynamical result. The choice of such a partition can sometimes be counterintuitive: For example, a low-frequency mode may not be treated classically if its coupling to the electronic states is large. Here, we discuss some examples of these convergence tests for the population dynamics, $P(t)$, in the RuFe system. Implicit for all the examples in this paper, the core always contains the electronic states.

Figure 3a displays $P(t)$ for the RuFe system at $T = 300$ K versus the number of higher frequency bath modes included in the core. For simplicity, the convergence with respect to the intramolecular core modes is shown with all outer-sphere solvent modes treated classically. It can be seen that the classical Ehrenfest model, where only the electronic states are treated quantum mechanically and all the bath modes (intramolecular plus solvent) are treated classically, predicts both a too-slow initial decay and an incorrect long-time limit for $P(t)$. Including some higher frequency intramolecular modes in the core improves the results to a certain extent. However, even with seven out of nine intramolecular modes in the core, the results are still unconverged within our 10% relative error criterion. Thus, for a numerically exact calculation of $P(t)$, all nine intramolecular modes have to be treated in the core part.

Due to the relatively weak coupling to the electronic states, less effort is required for the convergence of the outer-sphere solvent modes. This is true for both the number of configurations, as was demonstrated in the previous subsection, and the percentage of the modes included in the core. Figure 3b shows $P(t)$ with respect to the percentage of the solvent modes which are (together with all nine intramolecular modes) included in the core. Apparently, treating all the solvent modes classically (0% in the core) already gives reasonable results, although including 10% solvent modes in the core produces more accurate results with respect to our convergence criteria.

Thus in our self-consistent hybrid simulation of $P(t)$ for the RuFe system, the core part contains all nine intramolecular modes and 10% solvent modes (at $T = 300$ K). The relative size of the quantum core is similar for the RuRu system. We

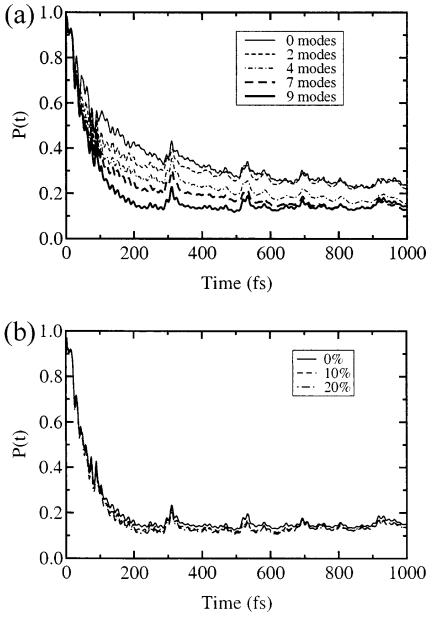

Figure 3. Convergence in the simulation of $P(t)$ at $T = 300$ K for the RuFe system. The reservoir modes are treated classically with the initial condition given by the corresponding Wigner distribution (see text). Twenty SP functions are used for each SP group of intramolecular modes and three SP functions for each SP group of solvent modes (in panel b). (a) $P(t)$ with respect to the number of intramolecular modes in the core (starting from the high-frequency end in Table 2), where all solvent modes are put in the reservoir; (b) $P(t)$ with respect to the percentage of the solvent modes in the core in addition to all nine intramolecular modes.

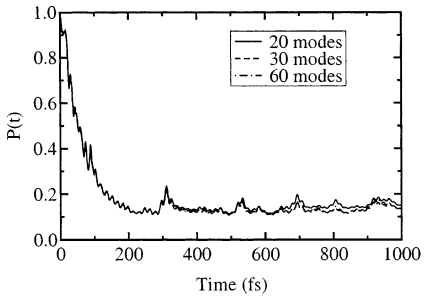

Figure 4. Convergence in the simulation of $P(t)$ at $T = 300$ K for the RuFe system with respect to the number of modes used to discretize the outer-sphere solvent bath.

note that such convergence depends on the couplings and time scales of the solvent modes, which will change if the solvent properties are changed. Furthermore, at low temperatures relatively more solvent modes need to be included in the core whereas at higher temperature the core size becomes smaller.

3. Convergence versus the Number of Solvent Modes. Due to the strong interactions between the intramolecular modes and the electronic states, the dynamical impact of the solvent is relatively weak for the systems considered in this work. Thus, unlike previous applications[50,51] to ET systems where only outer sphere baths are considered, a moderate number of modes is sufficient here to represent the continuous solvent. Figure 4 shows $P(t)$ for the RuFe system at $T = 300$ K with respect to the number of discrete modes used to represent the solvent. It is seen that 30−50 modes provide an adequate description for the overall ET dynamics. This number of modes has also been used in the calculations reported below. The relatively small number of modes needed to obtain converged results indicates that the intramolecular degrees of freedom play the most important role in the ET dynamics for the mixed-valence systems considered in this paper, whereas the effect of the solvent is on a more average level. More detailed discussions of this issue will be presented in the following section.

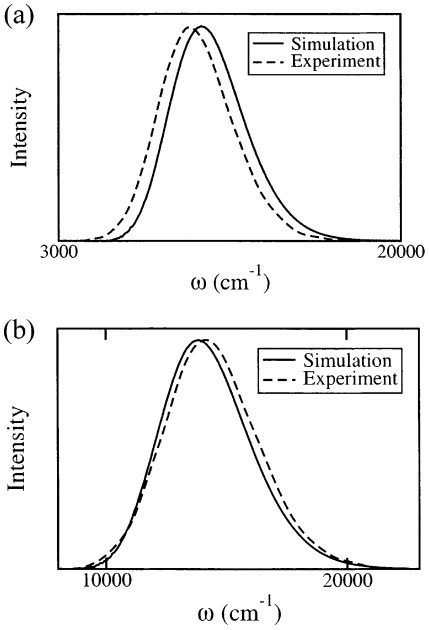

Figure 5. Comparison of simulated and experimental absorption spectra at room temperature for (a) RuFe compound in D_2O and (b) RuRu compound in D_2O. The experimental results are adapted from ref 15. Both spectra have been normalized.

IV. Results and Discussion

In this section we present results of simulations of the ET dynamics for the RuFe and RuRu systems. Unless specified otherwise, we have used the model parameters described in section II, i.e., those displayed in Tables 1 and 2 for the intramolecular modes, as well as solvent reorganization energies $\lambda_G = 2240$ cm^{-1} and $\lambda_D = 960$ cm^{-1}, and solvent relaxation parameters $\omega_G = 100$ cm^{-1} and $\omega_D = 10$ cm^{-1} corresponding to relaxation times $\tau_G \approx 53$ fs and $\tau_D \approx 530$ fs, respectively.

Since the parameters of our phenomenological model are based on the line-shape analysis of experimental absorption and resonance Raman spectra, it is illustrative to first compare the absorption spectra obtained from our self-consistent hybrid simulations with the experimental results[4] for the RuFe/RuRu compound in D_2O. The theoretical absorption spectra are obtained from Fourier transform of the corresponding dipole correlation functions, eqs 3.7 and 3.8. As shown in Figure 5, the overall agreement is quite good for the RuFe and RuRu systems. In both cases there are energy shifts between the simulated and the experimental spectra. These energy shifts are related to the fact that the "experimental" parameters used in our model have been obtained by fitting the absorption and resonance Raman spectra using an approximation that neglects the ET process between the two electronic states.[15] In the theoretical simulation, on the other hand, the coupling between the two electronic states, which is responsible for the ET, is fully taken into account. Employing a perturbative treatment, Barbara and co-workers have demonstrated that including the nonadiabatic coupling results in an energy shift of the absorption spectrum,[15] in qualitative agreement with our simulations.

For the RuRu system, the difference between the simulated and the experimental spectrum is somewhat more pronounced: in particular the band shapes are also slightly different. This finding indicates that in reality more than two electronic states

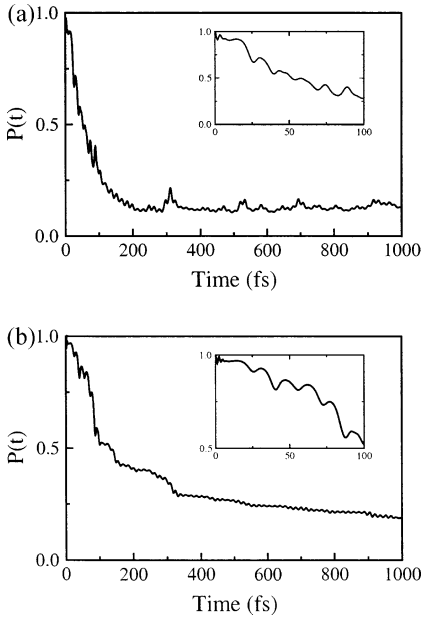

Figure 6. Time-dependent population of the charge-transfer state (at $T = 300$ K) for (a) the RuFe system and (b) the RuRu system. The insets show $P(t)$ for the first 100 fs.

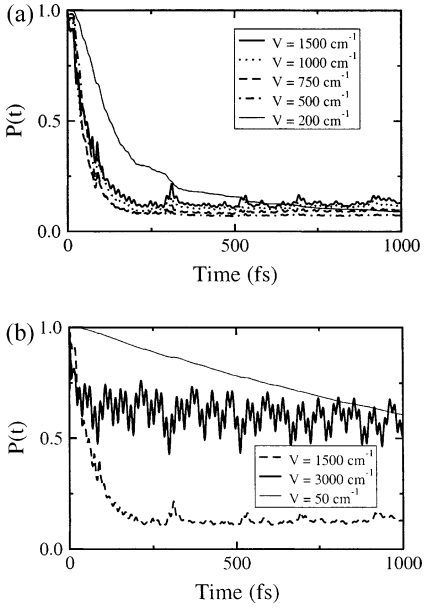

Figure 7. Dependence of the time-dependent population of the charge-transfer state on electronic coupling. The parameters used in the simulation are for the RuFe system, except that the electronic coupling V is varied from its default value.

might contribute to the MMCT band.[15,18,67] Furthermore, in the experimental fitting of the RuRu parameters the spin−orbit splitting of the ground state and the charge-transfer state was taken into account,[15] which was neglected in our simulation. It would be interesting to obtain a new set of parameters as well as including more electronic states that better reproduce the absorption spectra with our phenomenological model. This issue, together with theoretical simulations of pump−probe spectra for these intervalence ET reactions, will be addressed in future work.

The central result of this paper is the simulation of the dynamics of the back ET, which is directly reflected by the time-dependent population $P(t)$ of the charge-transfer state after photoexcitation. Figure 6 shows $P(t)$ for the RuFe and RuRu systems at $T = 300$ K. Overall, it is seen that both systems exhibit a fast back transfer of the electron. For the RuFe system the population decay of the charge-transfer state appears to be almost monotonic, for which an approximate exponential fit gives the relaxation time of ∼80 fs. Thus, as shown in Figure 6a, $P(t)$ reaches its average stationary value (of ∼90% ET) within a relatively short time (∼250 fs). In qualitative accordance with experimental results,[15] the back ET in the RuRu system is somewhat slower. In contrast to the RuFe system, the population of the charge-transfer state for the RuRu system, furthermore, exhibits an approximately bimodal decay character. Figure 6b shows that there is a fast component on a time scale of ≈120 fs which accounts for approximately 70% of the ET, and a slower component on the time scale of 1−2 ps. This bimodal decay for the RuRu system is in qualitative agreement with the experimental results of Barbara et al.[7,8,15]

Superimposed on the overall decay of the population of the charge-transfer state, oscillatory structures are observed. These structures are an indication of electronic and vibrational coherence effects. The separation of the coherence time scales is more easily seen for the RuRu system, Figure 6b. Here the overall time scale can be roughly divided into three groups: the frequency of the very fast oscillation, which can only be seen in the first 10 fs in the insert of Figure 6b, corresponds to the Rabi frequency of the bare electronic two-state system and is therefore a remnant of electronic coherence. The oscillations on a time scale of about 16 fs reflect the vibrational motion of the two high-frequency intramolecular modes included in the model (both high-frequency modes have been assigned to CN-stretch vibrations[19]). Finally, a steplike structure with a period of ≈200 fs can be seen. This period is close to the vibrational period of the strongly coupled intramolecular mode with frequency $\Omega_9 = 160$ cm^{-1} and has also been observed in the transient absorption spectra of Barbara and co-workers.[7,8] For the RuFe system, Figure 6a, the short-time electronic coherence (quenched Rabi oscillation) and the longer time high-frequency vibrational coherence can also be seen. However, due to the different ET time scale and the different interactions between the electronic and nuclear degrees of freedom, there is no clear indication of the vibrational coherence for the low-frequency ($\Omega_9 = 160$ cm^{-1}) mode.

To obtain a better understanding of the nature of the ET dynamics for the mixed-valence systems considered in this paper, let us investigate the dependence of $P(t)$ on the electronic coupling (V in eq 2.1). Figure 7 displays $P(t)$ for the RuFe system for several values of V at $T = 300$ K. It is well-known that in the nonadiabatic limit quantum perturbation theory (the golden rule) predicts that the ET time scale is inversely proportional to V^2. Such a perturbative treatment is clearly not applicable to the intervalence ET processes considered here. Figure 7a demonstrates that, within the range of $V = 500-1500$ cm^{-1}, the time scale of the population decay for the charge-transfer state is rather insensitive to the change in V. The major effect as V increases from 500 to 1500 cm^{-1} are the more-pronounced coherent structures superimposed on $P(t)$. Similar behavior has also been found for the RuRu system. This indicates that for the present mixed-valence systems the ET dynamics are influenced by nontrivial quantum interference effects between the electronic and nuclear degrees of freedom which cannot be described by approaches based on the quantum golden rule. Furthermore, our results demonstrate that the qualitative character of the population decay is, within a reasonable parameter range, rather insensitive to the electronic coupling V, suggesting the robustness of the model.

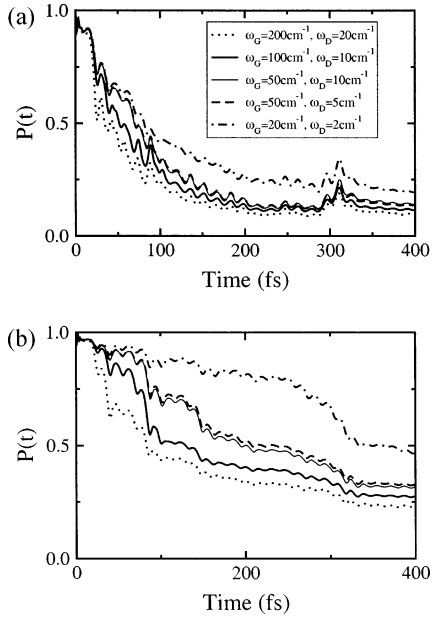

Figure 8. Dependence of the ET dynamics on the relaxation parameters of the solvent (a) for the RuFe system and (b) for the RuRu system. The different line properties represent $\omega_G = 200$ cm^{-1}, $\omega_D = 20$ cm^{-1} (dotted line); $\omega_G = 100$ cm^{-1}, $\omega_D = 10$ cm^{-1} (thick full line); $\omega_G = 50$ cm^{-1}, $\omega_D = 10$ cm^{-1} (thin full line); $\omega_G = 50$ cm^{-1}, $\omega_D = 5$ cm^{-1} (dashed line); and $\omega_G = 20$ cm^{-1}, $\omega_D = 2$ cm^{-1} (dashed−dotted line).

Figure 7 also shows that $P(t)$ undergoes significant changes if V reaches different limits. As V gets smaller, the population decay undergoes a transition to nonadiabatic ET. For $V = 200$ cm^{-1} (Figure 7a), not only the initial decay of $P(t)$ becomes slower, but it also shows bimodal behavior and a steplike structure (corresponding to the mode with frequency $\Omega_9 = 160$ cm^{-1}). As V gets even smaller, the nonadiabatic regime will eventually be reached and the ET process may be described by golden rule type approaches. This is illustrated for an electronic coupling of $V = 50$ cm^{-1} in Figure 7b. On the other hand, the ET process reaches the adiabatic limit as V increases. For example, Figure 7b shows that when V is increased to 3000 cm^{-1} the population exhibits partial localization with pronounced coherent structures superimposed on it.

The above results have been obtained with fixed values for the solvent parameters, chosen to mimic a fast relaxing solvent, such as D_2O or H_2O. Experimentally it has been found that the ET dynamics depend on the relaxation time scale of the solvent (dynamical solvent effect):[7] For the RuRu system the average ET time was found to increase from $\tau_{ET} \sim 100$ fs for water, as a fast relaxing solvent, to $\tau_{ET} \sim 220$ fs in the slower relaxing solvent ethylene glycol. Within our model, the relaxation time of the solvent is defined by the parameters τ_G (for the fast inertial decay) and τ_D (for the slower diffusive decay). Figure 8b illustrates that in qualitative agreement with experiment the ET in the RuRu system becomes slower for longer relaxation times of the solvent. This finding demonstrates that although the decay dynamics of the charge-transfer state is dominated by the influence of the intramolecular modes, the coupling to the solvent has a significant effect on the overall ET dynamics. The comparison in Figure 8b also shows that for the parameters considered here the dominant effect is caused by the Gaussian part of the solvent relaxation. The high-frequency part of the Debye spectral density has almost no effect on the fast initial decay ($t < 200$ fs), because the coupling strength concentrated in this part is negligible (cf. Figure 1). The dependence of the ET time scale on the solvent relaxation time is qualitatively

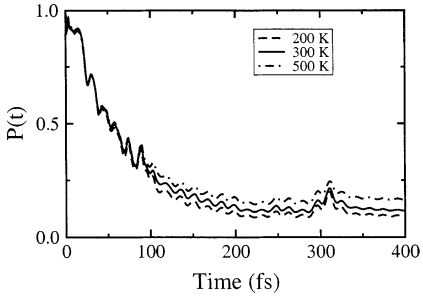

Figure 9. Dependence of ET dynamics on temperature for the RuFe system.

similar for the RuFe system, Figure 8a, although the change in τ_{ET} is much smaller compared with Figure 8b. This different dependence of the ET time scales on the solvent relaxation time is presumably a result of the faster initial decay of the charge-transfer state in RuFe; i.e., the bath cannot compete with such a fast ET process. As a result of this difference, the ET in RuRu should become significantly slower than in RuFe if a slower relaxing solvent is considered. This theoretical prediction is consistent with the experimental results: While the ET rates in RuRu and RuFe were found to be similar in fast relaxing solvents such as D_2O or H_2O,[10] in the slower relaxing solvent glycerol the ET process in the RuFe system is about 4 times as fast as that in the RuRu system.[15]

Another parameter of interest in ET processes is the temperature. Within our model we have found very weak dependence of the ET time scale on temperature in the range of 200−500 K for both systems, as illustrated in Figure 9 for RuFe. For the nonadiabatic ET regime, this is usually rationalized by the topology of the potential energy surfaces: If the ET occurs near the "activationless" regime (i.e., the crossing between the two diabatic surfaces is close to the minimum of the donor state), then the ET rate has a very weak dependence on the temperature. For the set of parameters used in the simulation, the energy minimum of the crossing between the two diabatic surfaces occurs, for both the RuRu and the RuFe systems, at less than 180 cm^{-1} above the minimum of the charge-transfer state. Therefore, the ET reaction is indeed close to the activationless regime. It should be noted, however, that the simulation also demonstrates that the ET reaction in RuRu/RuFe is not a simple rate process and therefore standard Marcus theory does not apply. Rather, the independence of temperature indicates that the ET process is strongly influenced by quantum interference effect between the electronic and the nuclear degrees of freedom, in particular the intramolecular modes.

Finally, it is important to point out that, due to the large electronic coupling and strong interactions between the electronic states and the inner-sphere modes in the intervalence ET systems considered here, many approximate methods will predict incorrect ET dynamics. To illustrate this, Figure 10 shows comparisons of self-consistent hybrid simulations of $P(t)$ with two commonly used approximations: the classical Ehrenfest model (classical path or TDSCF),[20−26] where all nuclear degrees of freedom are treated classically, and the noninteracting blip approximation.[32] While these approximations may be satisfactory for certain regimes, they are not applicable to the reactions considered in this paper. Figure 10 shows that for both RuFe and RuRu systems the classical Ehrenfest method predicts too slow an initial decay of the charge-transfer state as well as an incorrect long-time limit for $P(t)$. Furthermore, the classical Ehrenfest method completely misses the bimodal character of the population decay for the RuRu system. As already demonstrated in detail in the discussion of the convergence of the self-

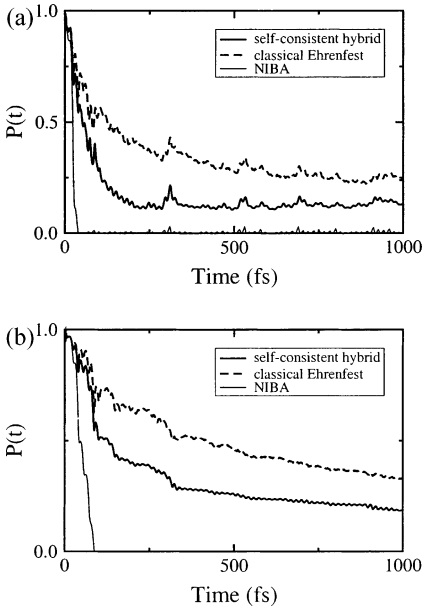

Figure 10. Comparison of dynamics of $P(t)$ as obtained by the self-consistent hybrid method, the classical Ehrenfest method, and the noninteracting blip approximation (NIBA) (a) for the RuFe system and (b) for the RuRu system.

consistent hybrid method, all the intramolecular modes plus a certain percentage of the solvent modes (10−20%) need to be included in the core for an accurate quantum dynamical treatment of these two mixed-valence systems.

The noninteracting blip approximation (NIBA) is based on perturbation theory with respect to the coupling between the two electronic states, V, and usually (if the process under consideration is a rate process) predict a rate close to the quantum golden rule rate. The comparison in Figure 10 demonstrates that these types of approaches are clearly not applicable to the RuRu/RuFe reactions, for which they predict a much too fast ET. This is to be expected for the system under consideration because the interstate coupling is not in the perturbative regime ($V = 1500$ cm^{-1}). Redfield theory, another common approximation used to describe ET, is also not expected to give reliable results for the present model because the time scale of the bath is too slow compared to the intramolecular time scale.

V. Concluding Remarks

In this paper we have applied the self-consistent hybrid method to simulate photoinduced ET reactions of the $(NH_3)_5Ru^{III}NCRu^{II}(CN)_5^-$ (RuRu) and the $(NH_3)_5Ru^{III}NCFe^{II}(CN)_5^-$ (RuFe) compounds in solution. The phenomenological model used in our simulations is based on the analysis of experimental line shapes by Hupp, Barbara, and co-workers,[7,15,19] and includes both inner-sphere intramolecular modes of the mixed-valence compounds and the effect of the outer-sphere solvent. In detailed convergence tests we have demonstrated that the self-consistent hybrid method is able to accurately describe the ET dynamics in these systems. This is in contrast to approximate methods such as the classical Ehrenfest approach or golden rule type methods. Due to the wide range of time scales for the nuclear degrees of freedom and the relatively strong electronic coupling in the intervalence ET reactions considered here, these methods where shown to give incorrect results.

Overall our simulations predict a fast back transfer of the electron after photoexcitation for both RuFe and RuRu compounds in a fast relaxing solvent. Whereas for RuFe in a fast relaxing solvent the decay of the charge-transfer state is dominated by a single time scale ($\tau_{ET} \sim 80$ fs), the ET dynamics in RuRu is characterized by a bimodal decay of the charge-transfer state with a fast component on a time scale of $\approx$120 fs which accounts for approximately 70% of the ET, and a slower component on the time scale of 1−2 ps. In both compounds the ET becomes slower in a slower relaxing solvent. Since this dynamic solvent effect is more pronounced in RuRu, ET in RuFe is expected to be significantly faster than ET in RuRu in a slower relaxing solvent. These theoretical findings are in qualitative agreement with experimental results.[7,15,19]

The simulations also reveal that the ET process in the two mixed-valence compounds considered is dominated by the influence of the intramolecular modes. The coupling to these inner-sphere modes results in oscillatory features superimposed on the population decay of the charge-transfer state, thus demonstrating the partially coherent nature of the ET process. It should be noted, however, that most of the electronic and vibrational coherent structures found in our simulation are on a relatively short time scale ($<$20 fs) and, therefore, are presumably difficult to observe experimentally.

We have, furthermore, studied in some detail the dependence of the ET dynamics on several physical parameters. Thereby it was found that the ultrafast dynamics of the back ET is almost independent of temperature and, within a reasonable parameter range, is relatively insensitive to changes in the strength of the electronic coupling. The latter finding suggests the robustness of the model and again demonstrates the inapplicability of golden rule type approaches.

In the present work we have focused on the population decay of the charge-transfer state, thereby assuming an instantaneous excitation, with an ultrafast laser pulse, from the electronic ground state. Although this population decay reflects the dynamics of the back ET, it is not straightforwardly measured experimentally. To have a more direct comparison with experimental pump−probe spectra, it is necessary to include the finite-duration laser pulse in the simulation. The self-consistent hybrid method needs to be generalized to directly simulate the nonlinear optical response to such a laser field. To facilitate the interpretation of the overall ET process, it is also important to examine other dynamical observables, e.g., the wave packet motion of the vibrational degrees of freedom. More work is currently being done along this direction to explore the complex interplay between ET dynamics, vibrational coherence, and solvent relaxation.

Acknowledgment. H.W. thanks New Mexico State University for the startup funds and the National Energy Research Scientific Computing Center (NERSC) for a generous allocation of supercomputing time. M.T. thanks W. Domcke for numerous helpful discussions and his continuous support.

References and Notes

(1) Marcus, R. A.; Sutin, N. *Biochim. Biophys. Acta* **1985**, *811*, 265.

(2) *Electron Transfer: From Isolated Molecules to Biomolecules*; Adv. Chem. Phys. 106−107; Jortner, J., Bixon, M., Eds.; Wiley: New York, 1999.

(3) Barbara, P. F.; Meyer, T. J.; Ratner, M. A. *J. Phys. Chem.* **1996**, *100*, 13148.

(4) Barbara, P. F.; Walker, G. C.; Smith, T. P. *Science* **1992**, *256*, 975.

(5) Dorn, S. K.; Dyer, R. B.; Stoutland, P. O.; Woodruff, W. H. *J. Am. Chem. Soc.* **1993**, *115*, 6398.

(6) Rubtsov, I. V.; Yoshihara, K. *J. Phys. Chem. A* **1999**, *103*, 10202.

(7) Kambhampati, P.; Song, D. H.; Kee, T. W.; Barbara, P. F. *J. Phys. Chem. A* **2000**, *104*, 10637.

(8) Song, D. H.; Kambhampati, P.; Kee, T. W.; Barbara, P. F. *J. Phys. Chem. A* **2002**, *106*, 4591.
(9) Vos, M. H.; Rappaport, F.; Lambry, J.-C.; Breton, J.; Martin, J.-L. *Nature* **1993**, *363*, 320.
(10) Reid, P. J.; Silva, C.; Barbara, P. F.; Karki, L.; Hupp, J. T. *J. Phys. Chem.* **1995**, *99*, 2609.
(11) Wynne, K.; Reid, G. D.; Hochstrasser, R. M. *J. Chem. Phys.* **1996**, *105*, 2287.
(12) Seel, M.; Engleitner, S.; Zinth, W. *Chem. Phys. Lett.* **1997**, *275*, 363.
(13) Wolfseder, B.; Seidner, L.; Stock, G.; Domcke, W.; Seel, M.; Engleitner, S.; Zinth, W. *Chem. Phys.* **1998**, *233*, 323.
(14) Walker, G. C.; Barbara, P. F.; Doorn, S. K.; Dong, Y.; Hupp, J. T. *J. Phys. Chem.* **1991**, *95*, 5712.
(15) Tominaga, K.; Kliner, D. A. V.; Johnson, A. E.; Levinger, N. E.; Barbara, P. F. *J. Chem. Phys.* **1993**, *98*, 1228.
(16) Wang, C.; Mohney, B. K.; Williams, R. D.; Petrov, V.; Hupp, J. T.; Walker, G. C. *J. Am. Chem. Soc.* **1998**, *120*, 5848.
(17) Vance, F. W.; Karki, L.; Reigle, J. K.; Hupp, J. T.; Ratner, M. A. *J. Phys. Chem. A* **1998**, *102*, 8320.
(18) Wang, C.; Mohney, B. K.; Akhremitchev, B. B.; Walker, G. C. *J. Phys. Chem. A* **2000**, *104*, 4314.
(19) Doorn, S. K.; Hupp, J. T. *J. Am. Chem. Soc.* **1989**, *111*, 1142.
(20) Mott, N. F. *Proc. Cambridge Philos. Soc.* **1931**, *27*, 553.
(21) Delos, J. B.; Thorson, W. R. *Phys. Rev. A* **1972**, *6*, 720.
(22) (a) Billing, G. D. *Chem. Phys. Lett.* **1975**, *30*, 391. (b) Billing, G. D. *J. Chem. Phys.* **1993**, *99*, 5849.
(23) (a) Gerber, R. B.; Buch, V.; Ratner, M. A. *J. Chem. Phys.* **1982**, *77*, 3022. (b) Buch, V.; Gerber, R. B.; Ratner, M. A. *Chem. Phys. Lett.* **1983**, *101*, 44.
(24) Micha, D. A. *J. Chem. Phys.* **1983**, *78*, 7138.
(25) Graham, R.; Höhnerbach, M. *Z. Phys. B* **1984**, *57*, 233.
(26) Stock, G. *J. Chem. Phys.* **1995**, *103*, 1561.
(27) (a) Preston, R. K.; Tully, J. C. *J. Chem. Phys.* **1971**, *54*, 4297. (b) Preston, R. K.; Tully, J. C. *J. Chem. Phys.* **1971**, *55*, 562. (c) Tully, J. C. *J. Chem. Phys.* **1990**, *93*, 1061.
(28) Herman, M. F. *J. Chem. Phys.* **1982**, *76*, 2949.
(29) Webster, F. J.; Rossky, P. J.; Friesner, R. A. *Comput. Phys. Commun.* **1991**, *63*, 494.
(30) Chapman, S. *Adv. Chem. Phys.* **1992**, *82*, 423.
(31) Leggett, A. J.; Chakravarty, S.; Dorsey, A. T.; Fisher, M. P.; Garg, A.; Zwerger, W. *Rev. Mod. Phys.* **1987**, *59*, 1.
(32) Weiss, U. *Quantum Dissipative Systems*; World Scientific: Singapore, 1999.
(33) Redfield, A. G. *Adv. Magn. Reson.* **1965**, *1*, 1.
(34) Jean, J. M.; Friesner, R. A.; Fleming, G. R. *J. Chem. Phys.* **1992**, *96*, 5827.
(35) May, V.; Kühn, O.; Schreiber, M. *J. Phys. Chem.* **1993**, *97*, 12591.
(36) Pollard, W. T.; Friesner, R. A. *J. Chem. Phys.* **1994**, *100*, 5054.
(37) Egorova, D.; Kühl, A.; Domcke, W. *Chem. Phys.* **2001**, *268*, 105.
(38) Kleinekathöfer, U.; Kondov, I.; Schreiber, M. *Chem. Phys.* **2001**, *268*, 121.
(39) Feynman, R. P.; Vernon, A. R. *Ann. Phys.* **1963**, *24*, 118.
(40) Coalson, R. D. *J. Chem. Phys.* **1987**, *86*, 995.
(41) Mak, C. H.; Chandler, D. *Phys. Rev. A* **1991**, *44*, 2352.
(42) Egger, R.; Weiss, U. *Z. Phys. B* **1992**, *89*, 97.
(43) Egger, R.; Mak, C. H. *Phys. Rev. B* **1994**, *50*, 15210.
(44) Makarov, D. E.; Makri, N. *Chem. Phys. Lett.* **1994**, *221*, 482.
(45) Makri, N.; Makarov, D. E. *J. Chem. Phys.* **1995**, *102*, 4600.
(46) Winterstetter, M.; Domcke, W. *Chem. Phys. Lett.* **1995**, *236*, 445.
(47) Stockburger, J.; Mak, C. H. *Phys. Rev. Lett.* **1998**, *80*, 2657.
(48) Evans, D. G.; Nitzan, A.; Ratner, M. A. *J. Chem. Phys.* **1998**, *108*, 6387.
(49) Thoss, M.; Wang, H. *Chem. Phys. Lett.* **2002**, *358*, 298.
(50) Wang, H.; Thoss, M.; Miller, W. H. *J. Chem. Phys.* **2001**, *115*, 2979.
(51) Thoss, M.; Wang, H.; Miller, W. H. *J. Chem. Phys.* **2001**, *115*, 2991.
(52) Sumi, H.; Marcus, R. A. *J. Chem. Phys.* **1986**, *84*, 4894.
(53) Jortner, J.; Bixon, M. *J. Chem. Phys.* **1988**, *88*, 176.
(54) In addition to the eight intramolecular modes used in the modeling in ref 15, we have included a ninth mode corresponding to a strongly coupled, low-frequency intramolecular mode that was observed recently in resonance Raman experiments; cf. refs 7 and 8.
(55) Chandler, D. In *Liquids, Freezing and Glass Transition*; Levesque, D., Hansen, J. P., Zinn-Justin, J., Eds.; Elsevier Science Publishers: Amsterdam, 1991.
(56) Bader, J. S.; Chandler, D. *Chem. Phys. Lett.* **1989**, *157*, 501.
(57) Schulten, K.; Tesch, M. *Chem. Phys.* **1991**, *158*, 421.
(58) Bader, J.; Chandler, D. *J. Chem. Phys.* **1992**, *99*, 4391.
(59) Jimenez, R.; Fleming, G. R.; Kumar, P. V.; Maroncelli, M. *Nature* **1994**, *369*, 471.
(60) Stratt, R. M.; Maroncelli, M. *J. Phys. Chem.* **1996**, *100*, 12981.
(61) The outer-sphere reorganization energy $\lambda_G + \lambda_D = 3200\ \mathrm{cm}^{-1}$ used in our simulation has been obtained from the parameters of Barbara et al. by subtracting the reorganization energy of the intramolecular mode with frequency $\Omega_9 = 160\ \mathrm{cm}^{-1}$ (which was not included in their model) from the reorganization energy of the bath to keep the total (inner sphere + outer sphere) reorganization energy fixed.
(62) Meyer, H.-D.; Manthe, U.; Cederbaum, L. S. *Chem. Phys. Lett.* **1990**, *165*, 73.
(63) Beck, M. H.; Jäckle, A.; Worth, G. A.; Meyer, H.-D. *Phys. Rep.* **2000**, *324*, 1.
(64) Wang, H. *J. Chem. Phys.* **2000**, *113*, 9948.
(65) (a) Wang, H.; Sun, X.; Miller, W. H. *J. Chem. Phys.* **1998**, *108*, 9726. (b) Sun, X.; Wang, H.; Miller, W. H. *J. Chem. Phys.* **1998**, *109*, 4190. (c) Sun, X.; Wang, H.; Miller, W. H. *J. Chem. Phys.* **1998**, *109*, 7064. (d) Wang, H.; Song, X.; Chandler, D.; Miller, W. H. *J. Chem. Phys.* **1999**, *110*, 4828.
(66) Bacić, Z.; Light, J. C. *J. Chem. Phys.* **1986**, *85*, 4594.
(67) Kober, E. M.; Goldsby, K. A.; Narayana, D. N. S.; Meyer, T. J. *J. Am. Chem. Soc.* **1983**, *105*, 4303.